FUEL-BASED THERMAL MANAGEMENT SYSTEM ARCHITECTURES AND TANK TEMPERATURE EVOLUTION MODELS FOR AVIATION

FUEL-BASED THERMAL MANAGEMENT SYSTEM ARCHITECTURES AND TANK TEMPERATURE EVOLUTION MODELS FOR AVIATION

S. Favre[1], F. Di Fede[2], E. Brusa[1] & C. Delprete[1]

[1]Politecnico di Torino, Corso Castelfidardo 39, Torino, 10129, TO, Italy
[2]Leonardo Labs, Leonardo SpA, Corso Castelfidardo 22, Torino, 10128, TO, Italy

Abstract

Thermal management system's (TMS) design has recently grown to become one of the main assets in the development of next generation aircraft, due to current trends favouring an increase in waste heat generation, especially in the context of propulsion and on-board systems electrification. Exploitation of intrinsic thermal capacity associated with conventional Jet-A fuel being stored in tanks appears as a promising solution to overcome such challenges. This paper aims to investigate the feasibility of said fuel-based TMS (F-TMS) in the context of propulsion electrification cooling, as well as presenting a modelling approach for the prediction of achievable thermal endurance. Two main cooling architectures are presented and compared, while preliminary investigation of heat rejection passively occurring through the tanks walls is also introduced. Finally, a generic, turboprop, regional transport aircraft is taken as a reference for the determination of the maximum achievable degree of hybrid-propulsion electrification to be managed via such architectures.

Keywords: Aircraft, Hybrid-electric, Thermal management, Fuel, Fuel cell

1. Introduction

The development of advanced thermal management systems (TMS) dedicated to the aviation sector has gained an ever-growing relevance over the last decades. Amongst several proposed solutions, designs exploiting the intrinsic heat capacity of tank-stored fuel have been investigated and discussed by many authors within the context of many different aerospace applications [1, 2, 3, 4]. The necessity to develop such systems firstly arose within military aviation to account for adequate electronics and components cooling[5, 6]. However, the prominence of this topic later spread also to the civil sector, as per the introduction of state of the art onboard electronics, the conceptualization and development of more electric aircraft, and even a recent rebirth in the interest towards supersonic and hypersonic flight, motivating the need for improved TMS solutions. Such later trends are also testified by the growing number of publications per year on the topic of aerospace TMS, as shown in Fig.1.

Within the context of clean aviation development, employment of fuel cells for power generation and propulsion electrification appears as most challenging subject, since the high amounts of generated waste heat, compounded by some relatively low operating temperatures, render adequate cooling hardly manageable by conventional architectures. Therefore, this paper aims to evaluate the feasibility of Fuel-based TMS (F-TMS), as a candidate cooling solution for next generation aircraft. A generic hybrid-electric, regional transport aircraft is hence taken as a reference for this study, in an effort to promote development of environmentally cleaner aviation.

2. State of art

Within the ample collection of documents provided by the literature and listed within Fig. 1 a high number of possible cooling solution are presented and discussed. Reviews by Van Heerden et al. [1], as well as Coutinho et al. [7], provide a complete and updated insight over all the prevalent topics concerning aviation TMS, ranging from F-TMS, surface mounted radiators and phase-change

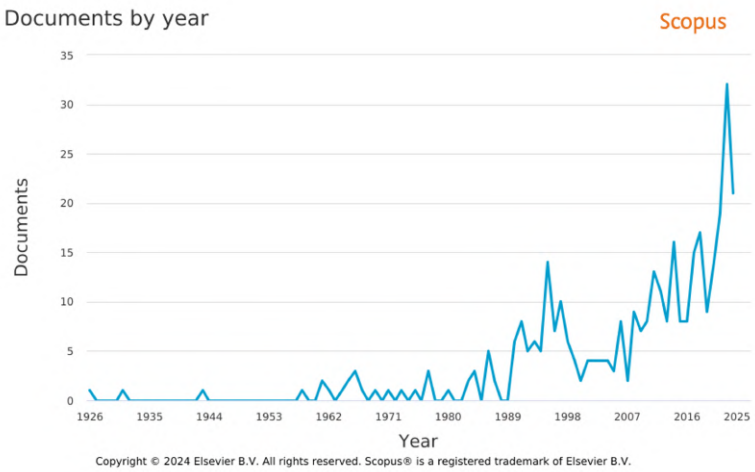

Figure 1 – Evolution of yearly publications numbers over the topic of aviation, fuel-based, TMS, up until Dec 2023. Provided by Scopus database.

materials, to the more conventional air-based designs. Amongst these, solutions exploiting intrinsic thermal inertia of fuel in tanks appear as a thriving subject, with studies ranging from military system cooling development [8, 2, 9, 10, 11, 12], to civil aviation thermal management [13, 14], aircraft electrification promotion [15, 16, 17], sustained supersonic and hypersonic flight achievement [18, 19], and even hybrid-rotorcrafts design [20].
Overall, most publications seem to focus over one of such themes: system level tank and cooling architectures definition and comparison [9, 10, 11, 12]; numerical CFD simulation of fuel behaviour inside tanks [8, 2]; and quantification of heat exchange phenomena through the tank surfaces [21, 15]. The work of Doman et al., in particular, provides an ample selection of documents concerning system level analysis [10, 11, 12, 22, 23, 24, 25] and testing [10] of F-TMS and the introduction of the "dual tank" architecture concept. The work of Kellermann et al. [15], on the other hand, places greater emphasis on the quantification of the heat exchange passively occurring between tank stored fuel and the external environment. Within this paper, the aim is to integrate the results of both studies, allowing for the prediction of fuel temperature dynamics and the evaluation of thermal endurance offered by the F-TMS, with respect to the employed architecture, as well as the presence of the heat rejection phenomenon occurring through the tank walls.
In the end, five main architectures can be found within the literature, and are here represented in Fig. 2. However, for the purpose of this paper, only the designs presenting a recirculation system will be taken into account, while dual and multi-tank designs will be left for future studies.

3. Use case

A generic, twin turboprop, regional transport aircraft is taken as a reference use case for the F-TMS modeling and simulation, in the evaluation of feasibility of the proposed architectures. Adequate cooling of a fuel cell power generation unit is defined as the main target of the thermal management system, within a broader context of efforts towards aircraft electrification and aviation sector carbon footprint reduction. In fact, due to typical efficiency of fuel cells hardly reaching values higher than 50%, generation of waste heat at least equal to the useful power being produced is to be expected and, thus, advanced cooling systems are also expected to be required. However, preservation of conventional propulsion units and fuel systems in the context of hybrid-electric aircraft development, justifies the presence and exploitation of fuel as a cooling system and is therefore discussed in the following pages.
Some typical regional transport aircraft parameters are: a passenger capacity ranging from 30 to 90 passengers (PAX), a total mechanical power going from 2.6MW to 8.2 MW, a maximum achievable range of about 1300km to 2000km, a most typical engine configuration being the twin-turboprop.

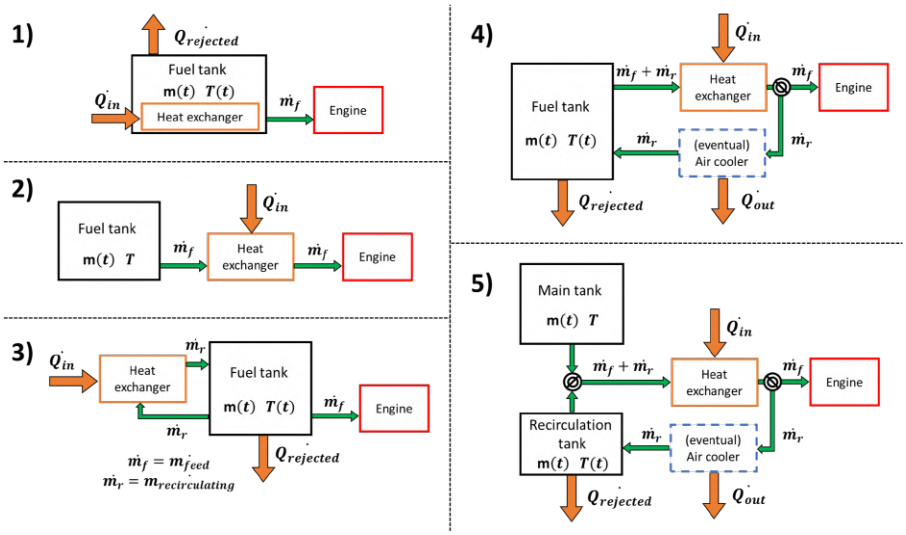

Figure 2 – Main fuel-based TMS architectures: 1) FTMS with submerged heat exchanger; 2) FTMS with direct feed heat exchangers; 3) FTMS with heat exchanger in parallel recirculation; 4) FTMS with heat exchanger in series recirculation; 5) FTMS with heat exchanger in series recirculation and double tank

4. Methodology

Modeling of the various elements composing the F-TMS is performed via the employment of the Eulerian formulation for open systems. A constant control volume is therefore defined and the associated parameters are evaluated with respect to their evolution over time. Some relevant hypotheses are also assumed while describing fuel internal properties. Homogeneous, isotropic and uniform behaviour are assumed for the fluid. A typical representation of the Eulerian formulation is provided in Fig. 3.

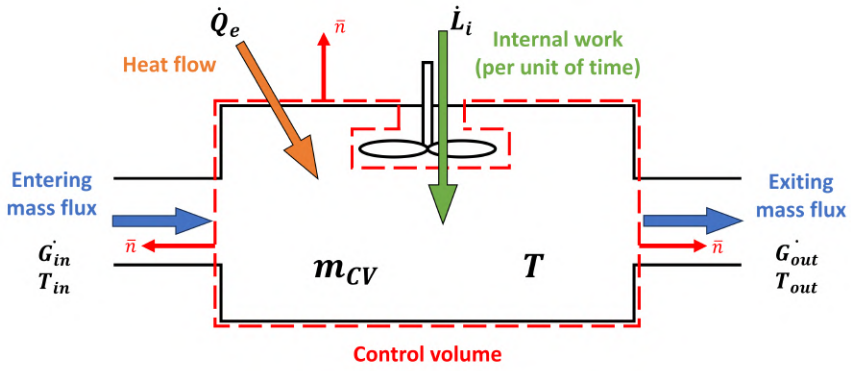

Figure 3 – Schematic representation of a thermodynamic system described via the Eulerian formulation.

4.1 Fuel tanks

The most relevant element within the entire F-TMS model is, arguably, the fuel tank component and the associated fuel mass. Two main physical properties are associated with this element: the instantaneously stored fuel mass, and the current fuel temperature value. Corresponding values of the fluid's density and temperature are assumed to be uniform in every point of the tank component, according to the previously stated hypothesis.

4.1.1 Dynamic mass behaviour modeling

Application of the Mass Conservation Law (MCL) (1) to the fuel tank boundaries allows for the determination of the fuel reserves progressive consumption and the consequent emptying dynamic of the

tanks.

$$\dot{m_{CV}} = \frac{dm_{CV}}{dt} = \sum_{i}^{n} G_i \tag{1}$$

Elicitation of the sum term into an exiting term and an entering one is possible. However, assuming that no refilling, or fuel transfer from other tank(s) is occurring, the latter is only ever present in the context of fuel recirculation. Therefore, the entering mass flow can be assumed to be equivalent to the recirculating mass flow, while the exiting mass flow can be set as equal to the recirculating mass flow plus the portion of fuel being currently burnt by the engines and, thus, ultimately consumed. Eq. (2) expresses this concept.

$$\frac{dm_{CV}}{dt} = G_{in} - G_{out} = (\cancel{G_{rec}}) - (G_{burnt} + \cancel{G_{rec}}) \tag{2}$$

Finally, Laplace transforms are applied to the previous formula, leading to eq.(3), and allowing for the implementation of the differential equations into the numerical model, developed via Simulink software.

$$s \cdot m_{CV} = G_{rec} - G_{burnt} - G_{rec} \tag{3}$$

4.1.2 Dynamic temperature behaviour modeling

Application of the First Law of Thermodynamics (FLT), in its Eulerian formulation (for open systems), instead, is taken as a reference for the determination of the fuel tank's thermal behaviour, eq.(4).

$$\dot{Q}_e + \dot{L}_i = \frac{d}{dt}\int_{V_{CV}} \rho \cdot (u + e_k + e_g + e_\omega)\, dV + \sum_{i}^{n}\left[\int_{A_i} \rho_i (h_i + e_{k,i} + e_{g,i} + e_{\omega,i})\vec{c}_i \cdot \vec{n}_i\, dS_i\right] \tag{4}$$

Pumps' introduced work is assumed to be negligible for the current level of abstraction. Therefore, the whole internal work term $\dot{L}_i$ is eliminated from the equation. Similarly, the gravitational e_g, kinetic e_k, and rotational e_ω energy terms are assumed not to vary significantly with respect to the chosen control volume and are, hence, also eliminated. Finally, application of the hypothesis of unidimensionality to the surface integral, as well as those of uniformity and homogeneity to the volume integral, allow for the FLT to be expressed as eq. (5).

$$\dot{Q}_e = \frac{d(u_{CV})}{dt} \cdot m_{CV} + u_{CV} \cdot \frac{d(m_{CV})}{dt} + \sum_{i}^{n} (h_i \cdot G_i) \tag{5}$$

Since the fluid of choice for this investigation is conventional Jet-A fuel, which is a kerosene-based combustible and, therefore, a liquid, both the enthalpy, as well as the internal energy variation over time, can be expressed through eq. (6). These considerations, in conjunction with the previously described Mass Conservation Law equation, eq. (2), lead to the simplified FLT formulation provided by eq. (7).

$$\frac{dh}{dt} \approx c_p \cdot \frac{dT}{dt} \approx \frac{du}{dt} \tag{6}$$

$$\dot{Q}_e = c_p \cdot m_{CV} \cdot \frac{dT_{CV}}{dt} + (h_{CV} - u_{CV}) \cdot G_{burnt} + (h_{CV} - h_{HE}) \cdot G_{rec} \tag{7}$$

Where h_{CV} represents the enthalpy of the actual fuel tank, and h_{HE} the enthalpy associated with the heated fuel exiting from the heat exchanger (HE) acting as the connection between the fuel system and the heat source. On the other hand, G_{burnt} represents the fuel flow being instantly consumed (by the engines), while G_{rec} describes the fuel flow being redirected back to the tank after having extracted heat from the heat source.

Absolute values of enthalpies with respect to the fluid temperature and internal energy are defined via eq. (8) and eq. (9), respectively. Application of said formulas to eq. (7), allows for further simplification of the FLT as of eq. (10).

$$h_{CV} - h_{HE} = c_p \cdot (T_{CV} - T_{HE}) \tag{8}$$

$$h = u + pv \tag{9}$$

$$\dot{Q}_e = c_p \cdot m_{CV} \cdot \frac{d(_{CV})}{dt} + (p_{CV} \cdot v_{CV}) \cdot G_{burnt} + c_p \cdot (T_{CV} - T_{HE}) \cdot G_{rec} \tag{10}$$

Finally, the remaining term $(p_{CV} \cdot v_{CV}) \cdot G_{burnt}$ is also neglected, representing, substantially, the work associated with fuel flow movement at the tank outlet. Such term, in fact, is generally associated with the presence of non-negligible internal work, however, having neglected any similar contribution, $(p_{CV} \cdot v_{CV}) \cdot G_{burnt}$ is also eliminated from the formula, providing eq. (11).

$$\frac{d(T_{CV})}{dt} = \dot{T_{CV}} = \frac{1}{m_{CV}} \cdot \left(\frac{\dot{Q}_e}{c_p} + G_{rec} \cdot (T_{HE} - T_{CV}) \right) \tag{11}$$

In conclusion, as in the case of the fuel mass dynamic, Laplace transforms are applied to equation (11) to translate the FLT formulation into a form best suited for dynamic numerical modelling, eq. (12). Within Simulink, in fact, the obtained temperature variation ratio $s \cdot T_{CV}$, can be later integrated to provide instantaneous temperature evolution $T_{CV}(t)$, given the initial temperature value.

$$s \cdot T_{CV} = \frac{1}{m_{CV}} \cdot \left(\frac{\dot{Q}_e}{c_p} + G_{rec} \cdot (T_{HE} - T_{CV}) \right) \tag{12}$$

A representation of the implementation of eq. (3), and eq. (12), into the numerical model is shown in Fig. 4. There, the fuel tank block is constructed by assuming the following parameters to be provided as inputs from other elements: the sum of all exchanged heat fluxes, both entering and exiting; as well as the sum of all entering and exiting fuel mass flows. On the other hand, the component is expected to provide real time evolution of tank stored mass and associated mean temperature.

A stop signal is also introduced to abruptly bring the simulation to an end whenever the instanta-

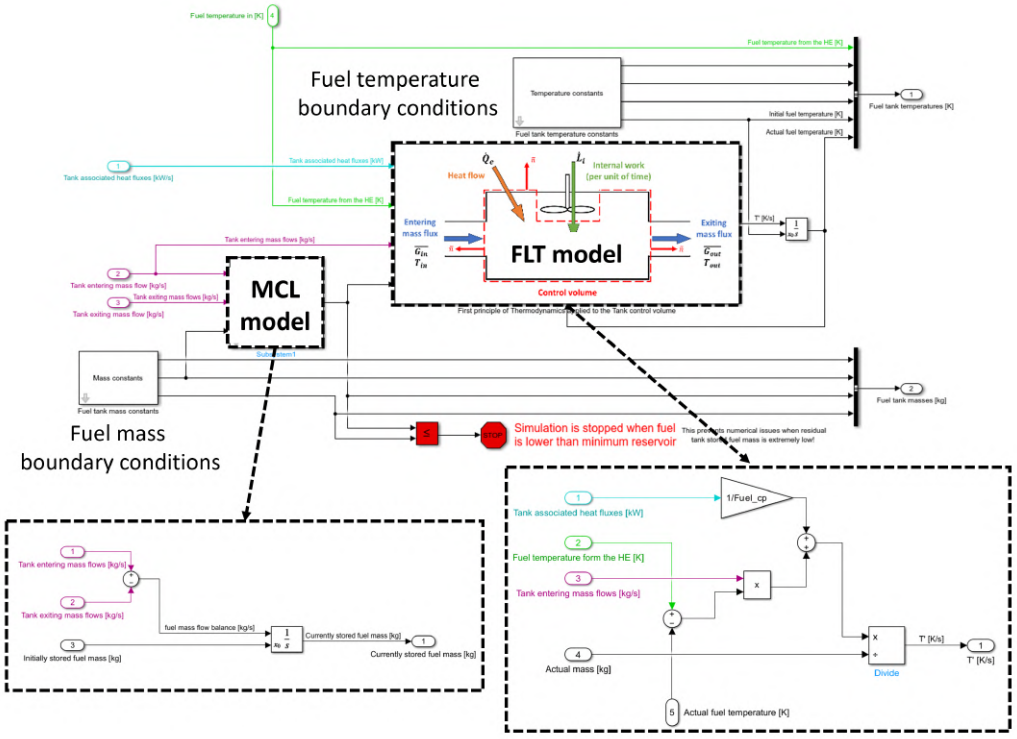

Figure 4 – Block model of fuel tank system neglecting heat rejection to the environment, and characterized by mass and thermal behaviour evaluation

neously stored fuel mass becomes lower than a predefined value, which, for the purpose of this study, is set at 5% of the maximum tank capacity. This is rendered necessary to prevent numerical errors

from interfering with the simulation whenever the actual fuel mass gets close to 0kg. Such a scenario, while "technically" possible is not expected to ever occur apart from some exceptional, major critical events which are not to be considered within the scope of this paper.

4.2 Engines

Within this study, engines are only associated with a mass transfer phenomena, since no heat exchange is expected to occur in such components that may influence other elements of the TMS. For this reason, the engine module is assumed as a simple, open, adiabatic system. In practice, the engines intervene within the simulation by introducing a fuel mass flow request G_{burnt}, which is provided as an input data to the tank's mass conservation law 2, with a negative sign with respect to the tank reference system. Value of this mass flux is provided as a time-variant input from a mission profile of choice.

4.3 Heat sources

Within this study, heat sources are only associated with a heat transfer phenomenon since no mass exchange is expected to occur in such components that may influence other elements of the TMS. For this reason, the heat source module is assumed as a simple, closed, diabatic system. In practice, the heat source(s) intervene within the simulation by introducing an entering heat flux $\dot{Q}_{HS}$ being imposed on the tank fuel mass through a heat exchanger component. The value of this heat flow is provided as a time-variant input from a mission profile of choice.

4.4 Heat exchanger

A heat exchanger component is defined in order to determine the required minimum fuel mass flow that allows for the adequate cooling of the heat source. No considerations are introduced regarding the heat exchanger efficiency, with the heat source temperature simply being assumed to always be about 5℃ higher than the maximum fluid temperature at the heat exchanger outlet. Thus, starting from the generalized Eulerian formulation of the FLT (4), it is possible to reduce said equation to the simplified form of eq. (7), via application of hypotheses analogous to those of section 4.1. Then, by assuming the cooling fuel flow request to not be subject to significant and rapid variations along the mission, the steady state hypothesis can also be introduced for the HE model. Hence, the two time-derivatives, $c_p \cdot \frac{dT}{dt} \cdot m$ and $u \cdot \frac{dm}{dt}$, can also be eliminated, leading to eq. (13), assuming the HE to only present one inlet and one outlet port.

$$\dot{Q}_e = h_{out} \cdot G_{out} - h_{in} \cdot G_{in} = c_p \cdot (T_{out} - T_{in}) \cdot G_{HE} \tag{13}$$

The required HE mass flow term G_{HE} can thus be extracted via equation (14). However, a maximum allowable mass flow threshold must also be set, since, according to the CS-25 regulation [26], local velocities of fuels cannot be higher than 6m/s within channels and plumbings. Consequently, the maximum allowable fuel mass flow is defined depending on the pipe cross-sectional areas of choice $G_{HE_{max}} = v_{max} \cdot A_{pipe_{cross-section}}$.

$$G_{HE} = \frac{\dot{Q}_e}{c_p \cdot (T_{out} - T_{in})} \tag{14}$$

Whenever the heat exchanger's required mass flow appears G_{HE} to be higher than the maximum achievable fuel flow $G_{HE_{max}}$, an insufficient cooling condition occurs, leading to the heat source temperature progressively growing beyond its nominal value. This phenomenon is modeled via equation (15), through rearrangement of eq. (13), and provides the corrected fuel outlet temperatures in insufficient cooling conditions.

$$T_{out} = T_{in} + \frac{\dot{Q}_e}{c_p \cdot G_{HE}} \tag{15}$$

The HE outlet fuel temperature so obtained represents a prevalent parameter in the determination of the fuel tanks' average temperature dynamics, while also acting as the driving factor in fuel natural convection computation in the heat rejection phenomena. Similarly, the HE required, and actually

provided, fuel mass flows are also relevant to the definition of both tank dynamics: the mass and the thermal one. However, concerning the HE employed fuel mass flow, some more in depth considerations have to be made with respect to the architecture of choice being employed. In fact, it is within the scope of this paper to compare the performance of two main architectures extracted from the representation in Fig. 2. Specifically the single tank recirculating-parallel and the recirculating-series ones are taken into account and discussed in the following lines.

4.4.1 Parallel recirculation.

In case of recirculating-parallel architectures, two separate paths are adopted in order to provide dedicated fuel flows to supply the engines or to cool the heat source. Therefore, the recirculating mass flow is the only one actively involved with the process of directly cooling the heat source, while the engines' consumed fuel mass flow is not. The value of the recirculating mass flow is thus coincident with the HE' required mass flow, up to saturation to its maximum value, according to eq. (16).

$$G_{rec} = G_{HE} \tag{16}$$

4.4.2 Series recirculation.

In case of recirculating-series architectures, however, the fuel is provided to both the HE and the engines via a single pipeline. The mass flux firstly passes through the heat exchanger(s), providing cooling to the heat source, yet is later split into one portion being required to feed the engines and the remaining portion being recirculated back to the fuel tank. However, in case the fuel flow request at the engines appears to be higher that that of the HE, no recirculating flow is to be expected since all tank exiting fuel is then provided to the engines. On the other hand, whenever the HE required mass flow exceeds the engines' burnt mass flow, the recirculating mass flow is defined as the difference between the HE required mass flow and the engine required mass flow, as can be seen from eq. (17).

$$\begin{cases} G_{rec} = 0 & \text{if } G_{engine} > G_{HE} \\ G_{rec} = G_{HE} - G_{engine} & \text{if } G_{engine} < G_{HE} \end{cases} \tag{17}$$

Clearly, independently from the configuration of choice, the tank consumed fuel mass flow is always equal to the engines' required fuel mass flow and does not necessarily coincide with the total exiting tank mass flow.

4.5 Heat rejection

Enhancement of the fuel tank component model can be achieved by eliminating the hypothesis of adiabatic system and introducing effects of heat rejection occurring through the tank walls. The fuel tanks, which are assumed to be placed inside the aircraft main wing, without a centre tank, can be approximated as a generic elongated prism of rectangular shape, and are here considered to only exchange heat through the lower horizontal tank surface. This is due to the fact that a significantly higher contribution is expected from this surface when compared to the others, which are either limited by small superficial extension or contact with non-flowing and/or gaseous fluids, which are known for relatively poor heat transfer performance. Hence, equation (18) is introduced to determine the heat flux being exchanged across the tanks' lowest surface, with an equivalent thermal resistance R_{eq} being defined as a series of two convective, and one conductive, thermal resistances, as in eq. (19)

$$\dot{Q} = \frac{A}{R_{eq}} \cdot \Delta T \tag{18}$$

$$R_{eq} = \sum_{i}^{n} (R_i) = \frac{1}{h_{air}} + \frac{L}{\lambda} + \frac{1}{h_{fuel}} \tag{19}$$

Where h_{air} is the convective heat exchange coefficient associated with the external environment (air). h_{fuel} is the convective heat exchange coefficient associated with the tank stored fuel. λ is the

conductive heat exchange coefficient of the tank walls (aluminum) with L being its respective width. λ is easily provided via tabular data correlating the parameter to the material of choice. On the other hand, definition of heat transfer coefficients of both fluids surrounding the tank wall, the external air, located below the surface, and heated fuel, collected above the surface, is much more complex.

4.5.1 Air convective heat transfer coefficient

Concerning the characterisation of the air associated heat transfer coefficient, it is reasonable to expect the heat exchange to both occur via natural as well as forced convection, since the relative velocity of the external airflow can vary significantly depending on the portion of the mission being performed: stand still, taxi, take off, climb, cruise, descent or landing. However, preliminary analysis evidenced the natural convection conditions to only provide minimal heat rejection, with negligible differences in the fuel tanks thermal dynamic when compared to adiabatic systems. Consequently, in order to achieve lower computational costs, the heat exchange has been assumed to only effectively occur whenever the external air was subject to forced convection. The Reynolds (20), Prandtl (21) and Nusselt numbers (22) are thus introduced for this investigation.

$$Re = \frac{\rho \cdot u \cdot L}{\mu} \tag{20}$$

$$Pr = \frac{c_p \cdot \mu}{\lambda} \tag{21}$$

$$Nu = f(Re, Pr) = \frac{h \cdot L}{\lambda} \tag{22}$$

Where the characteristic dimension of the heat exchange L is assumed to be the horizontal length of the fuel tank along the wing chord direction, and λ and h are the conductive and convective heat transfer coefficient of the external air, respectively. The Nusselt number formulations for a flat, isothermal, surface both in laminar (23), as well as in transition (24) and fully developed (25) turbulent flows were employed. The latter, seemingly being the prevalent condition thought a typical mission profile.

$$Nu = 0.664 \cdot Re^{1/2} \cdot Pr^{1/3} \qquad \text{if } Pr > 0.6,\ Re < 5 \cdot 10^5 \tag{23}$$

$$Nu = 0.037 \cdot \left(Re^{4/5} - 871\right) \cdot Pr^{1/3} \qquad \text{if } Pr > 0.6,\ Re \geq 5 \cdot 10^5 \tag{24}$$

$$Nu = 0.037 \cdot Re^{4/5} \cdot Pr^{1/3} \qquad \text{if } Pr > 0.6,\ Re \geq 5 \cdot 10^5 \tag{25}$$

In determining the external airflow temperature, normal day conditions are assumed, whilst dependence from altitude is derived according to the specifications of the International Standard Atmosphere, provided by atmosisa MATLAB toolbox. Finally, air temperature increase consequent to inertial compression and heating upon entering in contact with the aircraft surfaces is also accounted for via eq. (26).

$$T_{rec} = T_{inf}\left(1 + \frac{\gamma - 1}{2} \cdot \sqrt{Pr} \cdot Ma^2\right) \tag{26}$$

Where T_{rec} is the recovery temperature at the wing surface, and T_{inf} is the undisturbed air temperature at the defined altitude. $\gamma = \frac{c_p}{c_v}$ is the ratio between the air specific heat at constant pressure, and volume, respectively, while Ma is the instantaneous aircraft Mach number.

4.5.2 Fuel convective heat transfer coefficient

While determining the stored fuel heat transfer coefficient, instead, no significant forced flows are to be expected and natural convection is supposed to be prevalent. Hence, the necessary adimensional numbers become the already mentioned Prandtl (21) and Nusselt (22) numbers, as well as a newly introduced Grashof number (27), to be adopted in place of Reynolds in the Nusselt formula.

$$Gr = \frac{g \cdot L^3 \cdot \beta \cdot (T_{wall} - T_{inf})}{\left(\frac{\mu}{\rho}\right)^2} \tag{27}$$

Since the fuel temperature is almost certainly expected to be higher than that of the external air, cooling the tank floor, the most suitable natural convection formulation appears to be the one for a hot fluid ceding heat to a cold isothermal horizontal surface placed below the fluid itself. Unfortunately, with such a configuration, generation of natural convective motion is not favoured, with textbooks [27] suggesting that heat transfer solely occurs via conductive phenomena. Consequently, obtained heat rejection results minimal with such a layout, while differences in fuel temperature evolution appear with respect to an adiabatic system.
However, by assuming the fuel tank entering heat loads to be located close to the floor surface, the presence of a convective heat transfer phenomenon can be supposed, favoured by generation of localized hot fuel at the bottom of the tank. Such a configuration could be achieved either by placing a submerged HE close to the tank floor, as in one of the configurations proposed by Kellermann et al. [15], or by introducing a low lying "piccolo tube", supplying hot recirculating fuel from an external HE, as shown in Fig. 5. Therefore, the most suitable formulation for the formerly described conditions, seems to be the Nusselt equation for horizontal, isothermal hot plates placed below a generic cold fluid (28).

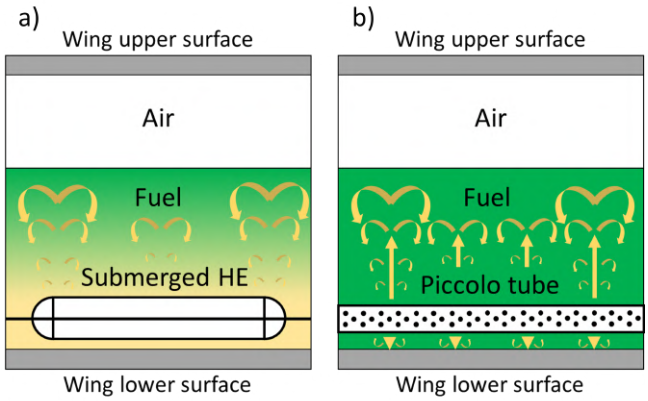

Figure 5 – Fuel natural convection being promoted via different means of heat introduction: a) via submerged heat exchanger placed at the bottom of the tank; b) via piccolo tube providing hot fuel mass flow at the bottom of the tank

$$\begin{cases} Nu = 0.54 \cdot Ra^{1/4} & \text{if } 10^4 < Ra < 10^7 \\ Nu = 0.15 \cdot Ra^{1/3} & \text{if } 10^7 < Ra < 10^{11} \end{cases} \tag{28}$$

Where the involved temperatures for the determination of the heat transfer coefficient are, thus, the average temperature of stored fuel T_{inf}, for the cold side, and the maximum temperature of fluid at the HE exit T_{wall}, for the hot side. Nevertheless, it is important to consider that equation (28) still represents an approximation of the actual behaviour occurring inside the tanks. Higher detail modeling, as well as specific tank geometry investigation, is advised for a better evaluation of the real fuel convective heat exchange coefficient.
The introduced heat rejection module expands the previously described tank component and receives as an input the instantaneous values of fuel temperature at the heat exchanger outlet, tank stored fuel mass, and associated average tank fuel temperature. On the other hand, the only output of this component is the currently rejected heat flux, which acts on the fuel tank's thermal submodel as an exiting heat flow. Representation of the heat rejection element model is provided in Fig. 6.

4.6 Mission profile

Finally, a mission planner component is also implemented to allow for reference mission profiles data to be uploaded into the model through .csv files, detailing the intended aircraft altitude, speed and rate of climb, with respect to each mission phase and its duration. Data concerning required mechanical power at the propellers, as well as the average engines' fuel consumption rates, are also introduced. The PW-127F turboprop engines performance spreadsheets [28, 29] being taken as a reference for this purpose and providing a conventional non-electric aircraft power to fuel consumption benchmark.

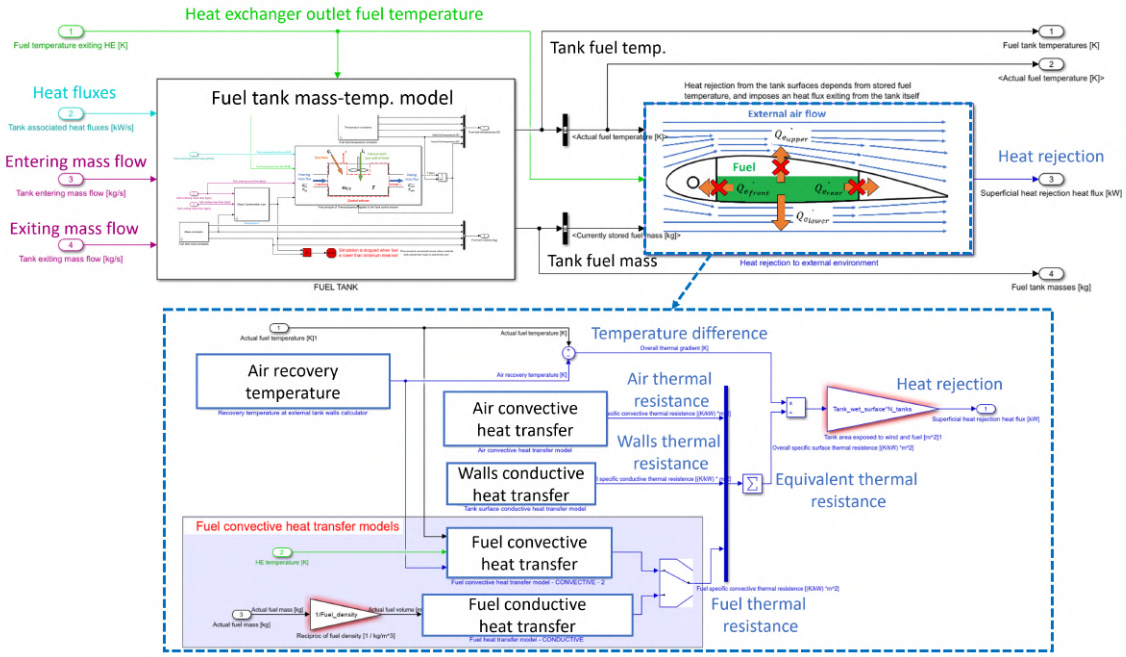

Figure 6 – Block model of a diabatic fuel tank system, characterized by an "internal" tank block and an interface heat rejection block (in blue)

These values are then exploited to determine fuel cell heat generation, as well as engines fuel consumption in the event of hybridization, assuming mechanical power request at the propeller remain constant. The power supply is thus split between conventional and electric portions, according to the desired degree of hybridization, while assumption that engines' fuel consumption could be scaled proportionally to their intended power output is employed. Therefore, the hybrid-electric aircraft fuel consumption is defined as in eq. (29), while the fuel cell generated waste heat is calculated through eq. (30).

$$G_{eng,tot} = (1 - H_d) \cdot P_{m,prop} \cdot N_{eng} \frac{G_{eng}}{P_{m,prop}} \tag{29}$$

Where $G_{eng,tot}$ is the total fuel being instantaneously burnt on the aircraft, H_d is the intended degree of hybridisation, expressed as the ratio between the mechanical power provided by the electric power unit with respect to the total required mechanical power $P_{m,el}/P_{m,prop}$. $P_{m,prop}$ is the required mechanical power at the propeller of one engine, and N_{eng} is the total number of engines present on the aircraft. Finally, $\frac{G_{eng}}{P_{m,prop}}$ represents the specific fuel consumption ratio of the reference PW-127F engine, which varies depending on the mission phase, and expresses fuel depletion with respect to required mechanical power at the propeller.

$$\dot{Q_{HS}} = H_d \cdot P_{m,prop} \cdot N_{eng} \frac{1}{\eta_{EM}} \frac{1}{\eta_{line}} \frac{1 - \eta_{FC}}{\eta_{FC}} \tag{30}$$

Where Q_{HS} expresses the total waste heat being instantaneously generated by the fuel cell, while H_d, $P_{m,prop}$, and N_{eng} are the same terms as in eq. (29). η_{EM}, η_{line}, and η_{FC}, instead, represent the electric motor, the electric line and the fuel cell nominal efficiencies, respectively.

4.7 Complete model

Through opportune connection of the interface ports of the various elements, the complete model is realized as represented in Fig. 7. An "option" block is finally introduced to allow for higher model flexibility, as well as automatic switching between different design conditions and architectures, allowing for iterative simulation.

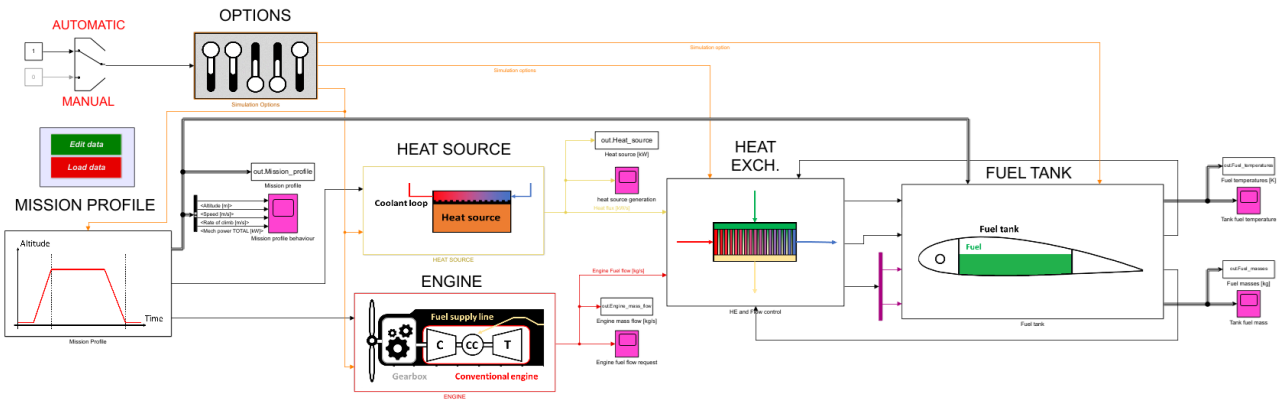

Figure 7 – Block model for the simulation of a F-TMS, its main components and interfaces.

5. Results

The described numerical model is here applied for the investigation of a F-TMS solution feasibility for a hybrid-electric, regional transport aircraft use case. Parameters comparable to those of some typical commercial regional transport aircraft [30, 31, 32], such as geometries, tank capacity, and materials are initialized into the model, as well as the Jet-A fuel and pure kerosene properties.

5.1 Cruise condition testing and parameter dependence

The first batch of simulations is intended to evaluate the TMS performance over a two hours' long cruise, characterized by reasonably constant engines' fuel consumption rates and fuel cells' heat generation. Coherently with typical regional turboprop aircraft specifications, the altitude is set to be equal to about 7600m, with an average speed of 500km/h. Concerning the heat source itself, a continuous heat flux generation of about 300kW is supposed, with a limit temperature of 100℃, which are reasonable values for a fuel cell-based, hybrid electric propulsion system with a low level of hybridization. The maximum processable heat exchanger fuel mass flow is then set to be equal to three times the typical engines fuel consumption ratio in cruise conditions. Finally, the initially stored fuel mass is assumed to be about 80% of the actual maximum tank capacity.
As simple recirculating-parallel architecture exhibiting adiabatic behaviour with respect to the external environment is employed for the determination of the following results.

5.1.1 Engine requirements

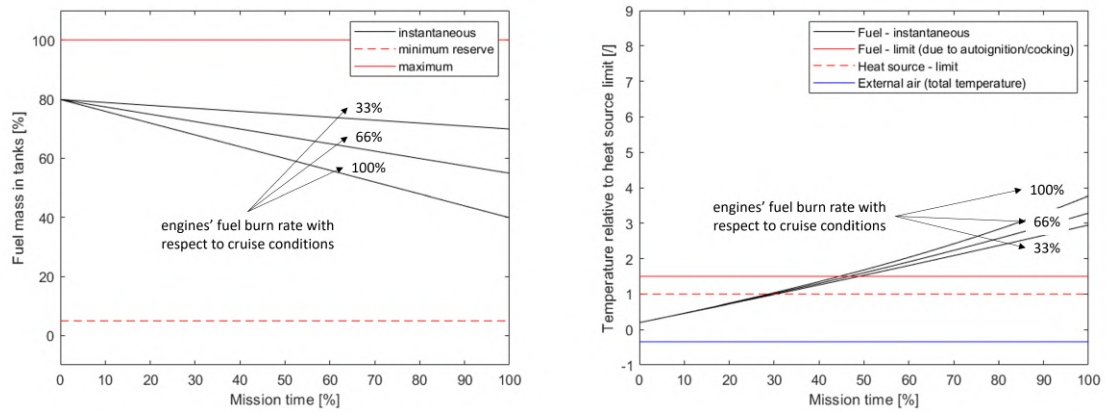

Figure 8 – Evolution of fuel tank properties according to the required engine feed fuel mass flow. Stored fuel mass is shown on the left, fuel temperature on the right.

Evaluation of the influence of the engine requirements over the fuel-TMS offered thermal endurance is achieved by varying the fuel mass consumption ratio required by said components, occurring, for

example, through downsizing of the conventional propulsion units in favour of electric ones. Results provided in Fig. 8 show how a tank's fuel mass and temperature evolution profiles are changed with the hypothesis of engines requiring only one third (33%), two thirds (66%), or the entirety (100%) of the typical fuel consumption rate in cruise conditions. Evidence of engines' required fuel mass flow rate increases leading to a faster depletion of available fuel reserves is in line with expectations. However, effects of faster storage depletion, also appear to result in augmented internal temperature rise rates. This is due to the fact that rapidly decreasing masses also reduce exploitable thermal inertia, thus favouring an earlier fault condition in the cooling system. In the end, however, due to the low operational temperature adopted for fuel cells, all cases resulted in exceeding the imposed temperature threshold prematurely, after completing about 28% of the intended mission duration.

5.1.2 Heat source requirements

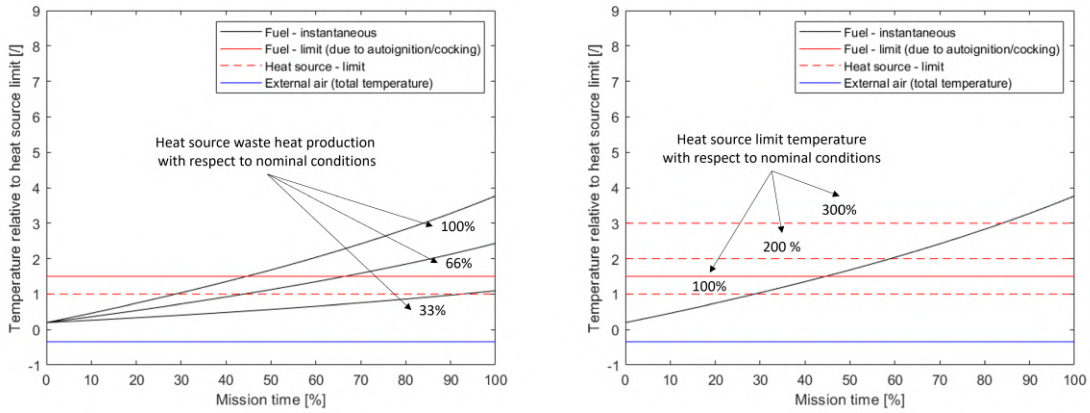

Figure 9 – Evolution of fuel tank temperatures according to the heat source imposed heat flux on the left. Evolution of fuel tank temperatures according to the heat source limit temperature on the right.

F-TMS performance investigations according to the amount of generated waste heat as well as maximum allowable heat source working temperature, are both performed and represented in Fig. 9. On the left portion of the image, fuel temperature evolution for three different heat loads of 300kW, 200kW and 100kW is shown, evidencing clear differences in overall system thermal endurance. The F-TMS, in fact, seems capable of providing adequate cooling to said heat sources only for about 28%, 44% and 92% of the intended mission profile, respectively. On the other hand, on the right portion of Fig. 9, F-TMS thermal endurance with respect to three different heat sources of 300kW each, yet presenting a maximum working temperature of 100 °C, 200 °C, and 300 °C respectively is presented. Results evidence that the TMS is capable of providing adequate cooling to said heat sources for about 28%, 58% and 84% of the intended mission profile respectively, thanks to temperature requirements relaxation.
However, it is also important to consider that some limitations also exists for appropriate fuel handling, whose temperature should not exceed 150 °C, in order to prevent, or at least minimize, chemical degradation of the hydrocarbons present in the kerosene mixture. Such a phenomenon takes the name of coking, and leads to the formation of solid precipitates within the fuel system which are responsible for nozzles, pumps and valves clogging, as well as significantly hindering heat transfer. Therefore, increases in heat sources allowable operating temperatures are only truly beneficial up to about 150 °C, unless some proper techniques are employed to prevent, or limit, the coking phenomena, such as special fuel mixtures and system cleaning devices. Hence, in the end, despite the 200 °C and 300 °C maximum temperature heat sources allowing for an improvement in the overall system thermal endurance up to 58% and 84% of the intended mission profile, the actual maximum coverage is constrained to about 45% due to temperature limitations associated with fuel handling, as evidenced by the continuous red line in Fig. 9.
Nevertheless, adoption of heat sources capable of managing temperatures higher than 150 °C is still to be considered a desirable feature in order to favour higher temperature deltas between the heat

source and the cooling fuel, thus reducing the need for high mass fuel flows and promoting heat exchanger compactness. However, special care shall be taken as, according to the CS-25 regulation [26], aircraft fuel shall only be in direct contact with surfaces at a temperature at least 50℃ lower than the fuel of choice's autoignition temperature, which, in the case of Jet-A fuel, is of about 225℃ to 230℃.

5.1.3 Architecture comparison

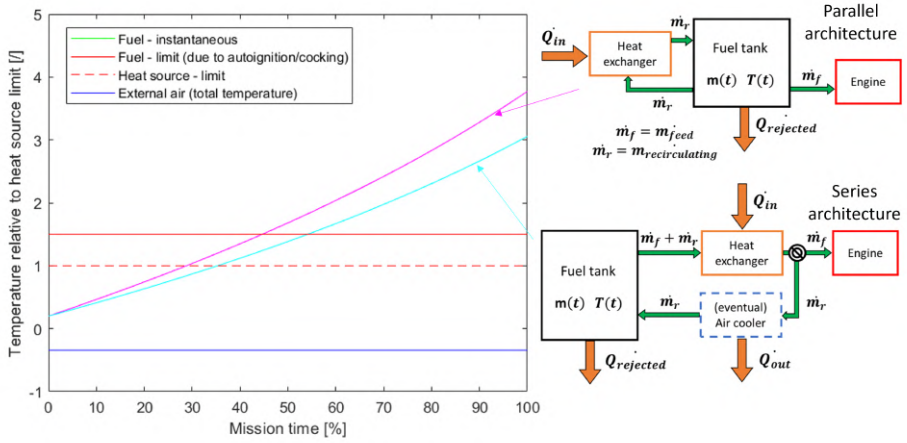

Figure 10 – Evolution of fuel tank temperatures in F-TMS architectures for adiabatic tank walls hypothesis.

The comparison between the thermal endurance offered by two different F-TMS architectures, the recirculating-parallel, and the recirculating-series one, is provided in Fig 10. Results evidence benefits of the recircualting-series architecture over the parallel one, with the former enhancing the predicted thermal endurance up to 35% of the total intended mission profile, from the latter previously presented 28%.
Obtained improvements in the overall aircraft thermal endurance are justified by the fact that, in a series architecture, fuel supply to the engines is always consumed after being heated to the maximum allowable temperature, unless the imposed heat load is very low and required cooling fuel mass flow is inferior to the one required by the engines. On the other hand, parallel configurations are bound to burn fuel at a temperature that is equal to that of the current average tank temperature. Said tank fuel temperature is inevitably lower than that of the heat source, and, thus, a portion of still available thermal capacity ends being burned in the engines, which could still have been employed to absorb heat from the heat source.

5.1.4 Heat rejection influence

Similarly to the previous case, influence of the heat rejection phenomena is provided both for the parallel and series configurations in Fig. 11. Results evidence that passive heat transfer from tank stored fuel to the external environment allows for significant improvement of the F-TMS' provided thermal endurance. The recirculating parallel architecture was able to extend its adequate cooling mission coverage from about 28% of the expected mission profile up to 65% of that same profile, by removal of the adiabatic walls hypothesis. Results of heat rejection introduction are even more prominent in the context of recirculating-series architectures, once again evidencing the benefits provided by such a design over a parallel one. This is well represented by the fact that such a configuration allows, for the first time, to achieve the full completion of the desired mission profile.
However, it is important to underline that, at this moment, performance of the heat excahngers is simplified and idealized. Introduction of realistic HE characterization will most certainly reduce said solution viability. Nevertheless, relevance of the heat rejection phenomena appears to be evident as well as consistent with the conclusions provided by Huang et al. [10].

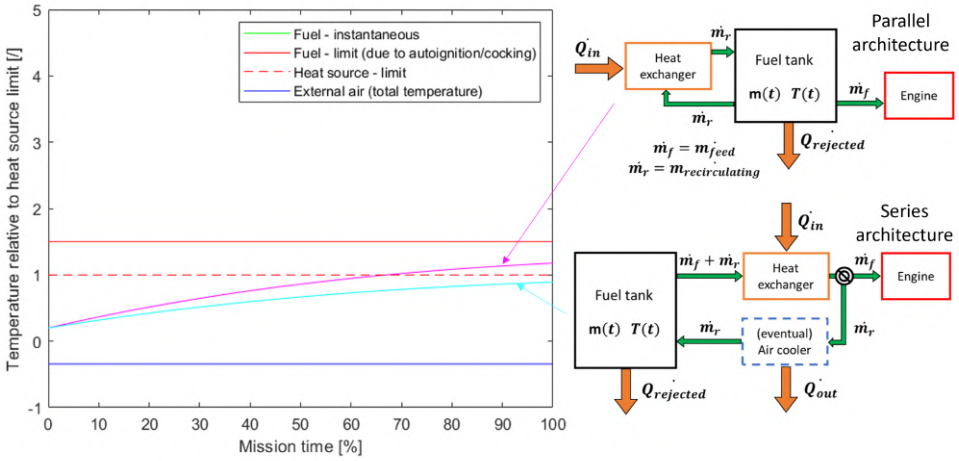

Figure 11 – Evolution of fuel tank temperatures in F-TMS architectures with convective fuel heat transfer through tank walls hypothesis.

5.2 Mission profiles

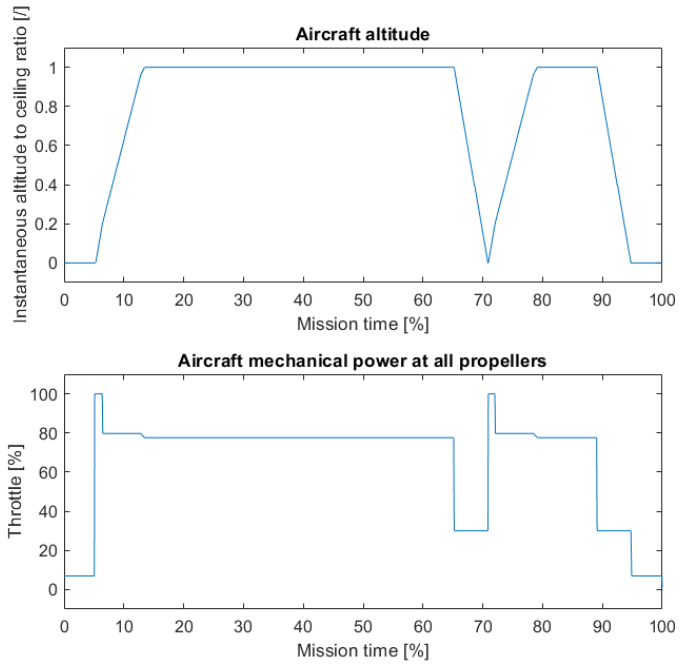

Figure 12 – Reference mission profile altitude (upper diagram) and mechanical power at the propeller (lower diagram).

Within this second batch of simulations, a complete mission profile with time-dependent altitude, speeds, fuel consumption and power demand is tested. The mission profile of choice is modeled after a worst case scenario where the aircraft is supposed to take off, climb, reach the maximum range in full payload conditions, descend, miss the approach and be forced to an alternate flight to the nearest available aerodrome at 250km from the original destination. A representation of the intended mission altitude with respect to the aircraft ceiling, as well as the percentage of instantaneously required mechanical power at the propellers is provided in Fig. 12.

5.2.1 Mass dynamics

The amount of tank stored fuel at the mission start is determined according to the specification of the EASA fuel implementation manual [33] assuming the total initial fuel mass to be expressed as eq. 31.

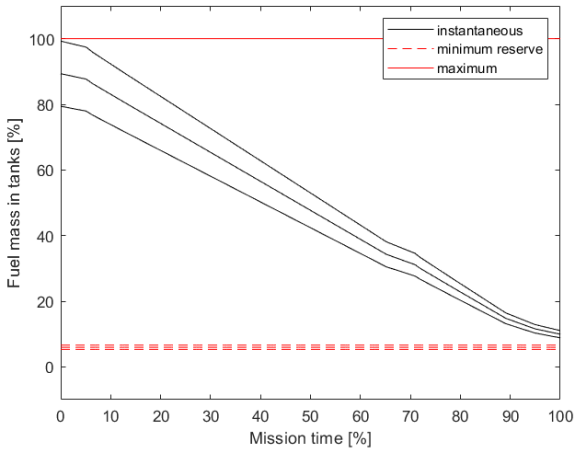

Figure 13 – Evolution of fuel tank masses for the reference mission profile with aircraft exhibiting different degrees of hybridization.

$$m_{f,0} = m_{f,taxi} + m_{f,trip} + m_{f,alt} + m_{f,cont} + + m_{f,fr} \tag{31}$$

Where $m_{f,0}$ is the required amount of fuel to be stored at the mission start, $m_{f,taxi}$ is the amount of fuel consumed during taxiing operations, $m_{f,trip}$ is the amount of fuel necessary for the completion of the scheduled journey, and $m_{f,alt}$ is the alternate fuel, which is equal to the amount of fuel necessary for the aircraft to reach cruising altitude after a missed approach, cruise to the next aerodrome and subsequently descend and land. The value of these last three terms is simply provided through integration of the fuel consumption ratio along the entirety of the intended mission profile. Finally, $m_{f,cont}$ represents the contingency fuel which is simply equal to 5% of the planned trip fuel consumption, and $m_{f,fr}$ is the final reserve fuel, which is equivalent to the amount of fuel necessary for the aircraft to cruise for 30min at altitude of 450m.
It is worth noting that, in the event of propulsion electrification, the reduced fuel consumption rate is automatically accounted for, via the implementation of eq. (29), which allows for the aircraft fuel mass to be minimized while still respecting regulations. This concept is evidenced in Fig. 13 where the amount of initially stored fuel is progressively diminished for increasing degrees of hybridization, 0%, 10%, and 20% specifically.

5.2.2 Thermal dynamics

Thermal dynamics simulation results for the previously stated levels of hybridization, 0%, 10% and 20%, are provided for the recirculating-parallel, as well as the recirculating-series architectures in Fig. 14, both including the effects of heat rejection phenomena. The presence of convective heat exchange occurring through the tanks is indicated by the fact that the configurations with a 0% degree of hybridization, and thus 0kW waste heat production, have their average fuel temperature depending solely on the external air temperature profile, which the system follows. It can also be seen that the performance of the series architecture is, once again, slightly superior when compared to that of the parallel architecture, especially during the initial phases of the mission.
Fig. 14 also evidences how progressive depletion of the fuel reserves leads to progressive diminishing of the temperature transitory time constant. This is particularly evident in the context of the second climb, where a high waste heat production, combined with a small residual thermal inertia, causes the fuel temperature to rise dramatically in a short period of time. This phenomenon, compounded by an already heated fuel reserve, causes the system to reach its peak registered fuel temperature at the end of the second climb phase.

5.2.3 Maximum hybridization degree

Finally, a simple iterative optimization was performed in order to select the maximum degree of hybridization achievable by the F-TMS without having the average fuel temperature ever exceed the

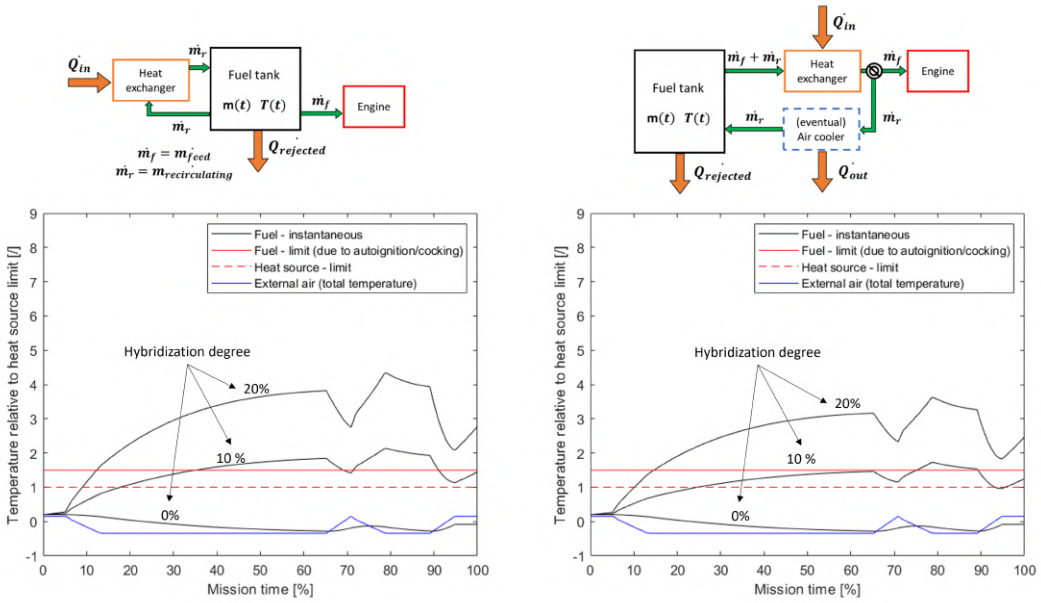

Figure 14 – Evolution of fuel tank temperatures for the reference mission profile with aircraft exhibiting different degrees of hybridization. Convective fuel heat transfer through tank walls hypothesis.

fuel cell limit temperature. Results of these iterations are provided in Fig. 15 both for parallel and series architectures. Once again, however, it is worth noting that, through a more in depth analysis of the HE performance, the effective maximum allowable degrees of hybridization is likely to be lower.

The obtained results show that the highest degree of hybridization achievable with the previously stated hypotheses are 4% for the parallel architectures and 6% for the series one. Unfortunately, current results are to be considered non-satisfactory in justifying the implementation of a similar design, and are a further evidence of the challenges associated with the management of the high waste heat generation associated with typical fuel cell operation.

Nevertheless, several interesting results were provided by these simulations, suggesting a number of different approaches that may be employed in order to increase the maximum achievable hybridization degree to some more compelling values. First of all, multiple evidences of the system's struggle in providing adequate cooling at the later stages of the mission were collected. Proper management of power sources could be introduced to enhance TMS effectiveness. This could be done by maximizing electric power generation only during the initial phases of the mission, when high available fuel thermal inertia allows for greater quantities of heat to be safely managed. Additionally, minimization of waste heat production during the later portions of the flight, such as the end of the cruise and descent, could be employed to favour heat rejection and faster recovery of exploitable thermal inertia in the event of a subsequent emergency climb. The nature of the heat rejection phenomena, then, has been introduced through a simplified formulation, only focusing on the heat transfer occurring through the lower tank walls and assuming some simplified internal fluid motion. However, even at such a high level of abstraction, advantages introduced by the preliminary evaluation of the heat rejection phenomenon appeared as a most promising asset in the system's thermal endurance improvement. Hence, further investigation of this topic involving higher detail modelling, design of convective heat transfer enhancement solutions, as well as F-TMS integration of with other architectures such as surface heat exchanges appears as a viable option. Finally, introduction of more complex architectures, such as the dual-tank, recirculating series design proposed by Doman et al. [24], may also further enhance the F-TMS performance.

6. Conclusion

The relevance of F-TMS and the drivers motivating their development are clear from the literature. A dynamic, system level model for preliminary investigation of fuel-based Thermal Management Sys-

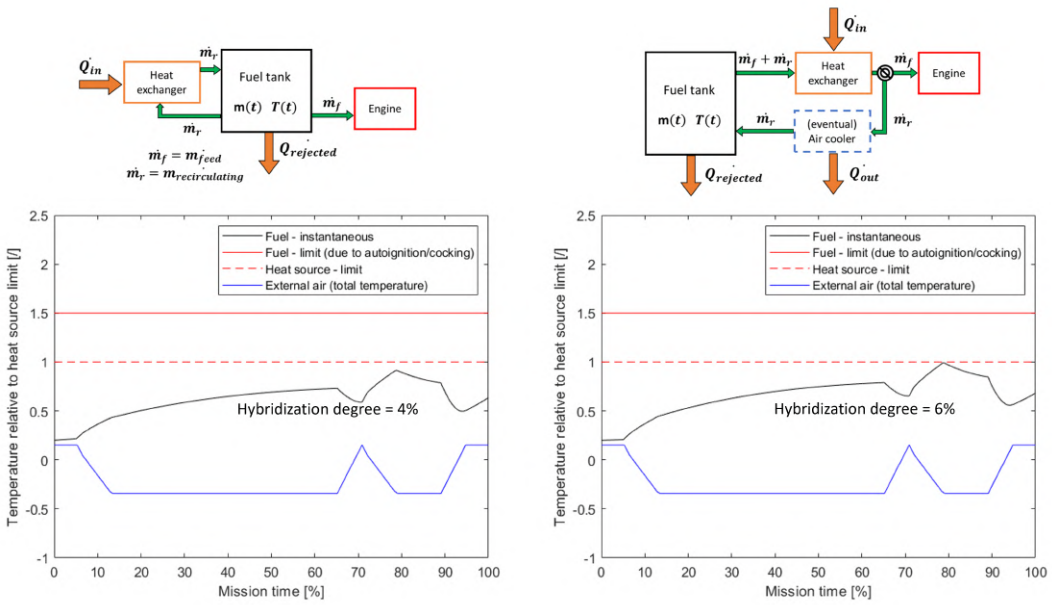

Figure 15 – Evolution of fuel tank temperatures for the reference mission profile with aircraft exhibiting different degrees of hybridization. Convective fuel heat transfer through tank walls hypothesis.

tems' performance in the context of hybrid-electric, regional transport aircraft development is here presented and discussed.

Relevance of several parameters in the determination of F-TMS feasibility in fuel cell driven hybrid-electric aircraft is evaluated. Analyses concerning the influence of fuel consumption rates and waste heat generation are performed, evidencing the progressive fuel thermal capacity erosion. Minimization of fuel burning ratios during the initial phases of the flight favouring electric power generation instead is therefore advised. On the other hand, limitation in the use of heat generating components, such as fuel cells, at the later phases of the mission is preferable, in favour of higher consumption rates, when the remaining fuel is both limited and hot.

Increases in the maximum allowable heat source temperature are proven to beneficial to the overall aircraft associated thermal endurance, via relaxation of some TMS requirements. However, due to fuel becoming subject to undesirable chemical reactions and coking at temperatures exceeding 150 ℃, said benefits are shown to only be exploitable up to such a threshold. Nevertheless, heat sources capable of managing temperatures higher than 150 ℃, are still preferable in order to favour higher temperature differences between the fuel cell and the fuel, thus preventing the need for high coolant mass flows and promoting heat exchanger compactness.

Preliminary investigation of heat rejection phenomena suggests this to be a high impact asset for overall improvement of the aircraft thermal endurance, with promising results being achieved despite the high level of abstraction adopted for preliminary modelling. A more in depth evaluation of the heat rejection mechanism, as well as the convective heat transfer coefficient is highly advisable.

Similarly, a comparison between recirculating-parallel and recirculating-series architectures is conducted, suggesting the latter to provide significantly better performance and being capable of managing roughly 20% to 30% more powerful heat sources. Implementation and comparison with higher complexity designs, such as the dual-tank system proposed by Doman et Al. [23, 22] should also be considered.

Finally, preliminary design optimization suggests the maximum achievable degrees of hybridization of the system to be around 4% and 6% for the parallel and series architectures respectively, assuming currently employed hypotheses. These results are to be considered non-satisfactory and are a further evidence of the challenges associated with the management of the significantly high amounts of waste heat being produced by typical fuel cell units. Nevertheless, a number of modifications, improvements and different approaches could still be employed in order to enhance the feasibility of the

F-TMS solution up to more compelling results. The introduction of wing longerons thermal conduction, the integration of all tank surfaces heat transfer, as well as a precise analysis of fuel convection could all prove beneficial to the overall F-TMS feasibility improvement. Furthermore, integration of more advanced architectures, their combination with other kinds of solutions, as well as development of proper mission design and fuel cell activity planning, are most likely to provide increases in the maximum manageable degree of hybridization.

Declaration of competing interests

The authors declare that they have no known competing financial interests or personal relationships that could have appeared to influence the work reported in this paper.

Acknowledgments

This publication is part of the project PNRR-NGEU which has received funding from the MUR - DM352/2022 (CUP n° E12B22000560006).

Contact Author

Stefano Favre, ORC-ID: 0009-0004-6540-4070, email: stefano.favre@polito.it

Copyright Statement

References

[1] A.S.J. van Heerden, D.M. Judt, S. Jafari, C.P. Lawson, T. Nikolaidis, and D. Bosak. Aircraft thermal management: Practices, technology, system architectures, future challenges, and opportunities. *Progress in Aerospace Sciences*, 2022.

[2] Y. Liu, G. Lin, J. Guo, and J. Zhu. Dynamic prediction of fuel temperature in aircraft fuel tanks based on surrogate. *Applied Thermal Engineering*, 2022.

[3] N. Heersema and R.H. Jansen. Thermal management system trade study for SUSAN electrofan aircraft. In *AIAA Science and Technology Forum and Exposition, AIAA SciTech Forum 2022*, 2022.

[4] W.G. Dukek. Supersonic jet fuels - quality and cost factors. 1961.

[5] William A. Hudson and Mark L. Levin. INTEGRATED AIRCRAFT FUEL THERMAL MANAGEMENT. In *Proceedings - Society of Automotive Engineers*, 1986.

[6] Edward P. Petkus and Roger W. Gallington. HALE thermal balance. In *AIAA/ASME/SAE/ASEE 23rd Joint Propulsion Conference, 1987*, 1987.

[7] Maria Coutinho, David Bento, Alain Souza, Rodrigo Cruz, Frederico Afonso, Fernando Lau, Afzal Suleman, Felipe R. Barbosa, Ricardo Gandolfi, Walter Affonso, Felipe I.K. Odaguil, Michelle F. Westin, Ricardo J.N. dos Reis, and Carlos R.I. da Silva. A review on the recent developments in thermal management systems for hybrid-electric aircraft. *Applied Thermal Engineering*, 2023.

[8] Y. Suat, A.D. Özkan, and E. Sirkeci. 1d modelling of thermal management of a jet trainer aircraft. In *SAE Technical Papers*, 2023.

[9] R. Manna, N. Ravikumar, S. Harrison, and K.G. Boulama. Aircraft fuel thermal management system and flight thermal endurance. *Transactions of the Canadian Society for Mechanical Engineering*, 2022.

[10] G.P. Huang, D.B. Doman, M.J. Rothenberger, B. Hencey, M.P. DeSimio, A. Tipton, and D.O. Sigthorsson. Dimensional analysis, modeling, and experimental validation of an aircraft fuel thermal management system. *Journal of Thermophysics and Heat Transfer*, 2019.

[11] M.W. Oppenheimer, D.O. Sigthorsson, and D.B. Doman. Control of fuel thermal management systems with transport delays. In *AIAA Scitech 2019 Forum*, 2019.

[12] D.B. Doman. Fuel flow topology and control for extending aircraft thermal endurance. In *Journal of Thermophysics and Heat Transfer*, 2018.

[13] A.S.J. van Heerden, D.M. Judt, C.P. Lawson, S. Jafari, T. Nikolaidis, and D. Bosak. Framework for integrated dynamic thermal simulation of future civil transport aircraft. In *AIAA Scitech 2020 Forum*, 2020.

[14] P. Abolmoali, A. Donovan, S.S. Patnaik, P. McCarthy, D. Dierker, N. Jones, and R. Buettner. Integrated propulsive and thermal management system design for optimal hybrid electric aircraft performance. In *2020 AIAA/IEEE Electric Aircraft Technologies Symposium, EATS 2020*, 2020.

[15] H. Kellermann, A.L. Habermann, P.C. Vratny, and M. Hornung. Assessment of fuel as alternative heat sink for future aircraft. *Applied Thermal Engineering*, 2020.

[16] D. Li, S. Dong, J. Wang, and Y. Li. Modeling and simulation of system-level temperature for airliner hydraulic system in a full flight mission profile. In *IET Conf Publ*, volume 2018, pages 338–343. Institution of Engineering and Technology, 2018.

[17] J.H. Kim, K.S. Kwon, S. Roy, E. Garcia, and D. Mavris. Megawatt-class turboelectric distributed propulsion, power, and thermal systems for aircraft. In *AIAA Aerospace Sciences Meeting, 2018*, 2018.

[18] T. Jia, X. Zhang, Y. Liu, S. Gong, C. Deng, L. Pan, and J.-J. Zou. A comprehensive review of the thermal oxidation stability of jet fuels. *Chemical Engineering Science*, 2021.

[19] Y. Feng, Y. Liu, Y. Cao, K. Gong, S. Liu, and J. Qin. Thermal management evaluation for advanced aero-engines using catalytic steam reforming of hydrocarbon fuels. *Energy*, 2020.

[20] I. Roumeliotis, L. Castro, S. Jafari, V. Pachidis, L. de Riberolles, O. Broca, and D. Unlu. Integrated systems simulation for assessing fuel thermal management capabilities for hybrid-electric rotorcraft. In *Proceedings of the ASME Turbo Expo*, 2020.

[21] Anaïs Luisa Habermann, Ankit Khot, David Emanuel Lampl, and Christof Perren. Aerodynamic effects of a wing surface heat exchanger. *Aerospace*, 10(5):407, April 2023.

[22] D.B. Doman. Fuel flow control for extending aircraft thermal endurance part II: Closed loop control. In *2016 AIAA Guidance, Navigation, and Control Conference*, 2016.

[23] D.B. Doman. Fuel flow control for extending aircraft thermal endurance part i: Underlying principles. In *2016 AIAA Guidance, Navigation, and Control Conference*, 2016.

[24] D.B. Doman. Optimal cruise altitude for aircraft thermal management. *Journal of Guidance, Control, and Dynamics*, 2015.

[25] D.B. Doman. Rapid mission planning for aircraft thermal management. In *AIAA Guidance, Navigation, and Control Conference, 2013*, 2015.

[26] Certification Specifications (CSs).

[27] T. L. Bergman, Adrienne Lavine, and Frank P. Incropera. *Fundamentals of heat and mass transfer*. John Wiley & Sons, Inc., Hoboken, NJ, eighth edition edition, 2017. OCLC: 964065461.

[28] EASA. Type-certificate data sheet. https://www.easa.europa.eu/en/downloads/7725/en.

[29] Atr: The optimum choice for a friendly environment. https://web.archive.org/web/20160808173542/http://web.fc.fi/data/files/ATR_TheOptimumChoice.pdf.

[30] Atr 72-600 brochure booklet. https://www.atr-aircraft.com/wp-content/uploads/2020/07/Factsheets_-_ATR_72-600.pdf.

[31] Dash 8-400 brochure booklet. https://dehavillandfield.com/wp-content/uploads/2022/08/Dash8_Spec_Sheet_web.pdf.

[32] Fokker 50 brochure booklet. https://www.fokkerservices.com/media/z05j5mhx/fokker50_informationbooklet.pdf.

[33] EASA. Fuel implementation manual. https://www.easa.europa.eu/community/system/files/2024-01/EASA-AESA%20Fuel%20implementation%20manual%20V0.3%2019.01.2024.pdf.